Precise and Long-Term Tracking of Adipose-Derived Stem Cells and Their Regenerative Capacity *via* Superb Bright and Stable Organic Nanodots

Dan Ding,[†,‡,⊗] Duo Mao,[†,⊗] Kai Li,[§,⊗] Xiaomin Wang,[†] Wei Qin,[∥] Rongrong Liu,[§] David Shunzhong Chiam,[‡,§] Nikodem Tomczak,[§,⊥] Zhimou Yang,[†] Ben Zhong Tang,[*,∥] Deling Kong,[*,†] and Bin Liu[*,‡,§]

[†]State Key Laboratory of Medicinal Chemical Biology, Key Laboratory of Bioactive Materials, Ministry of Education, College of Life Sciences, and Collaborative Innovation Center of Chemical Science and Engineering (Tianjin), Nankai University, Tianjin 300071, P. R. China, [‡]Department of Chemical and Biomolecular Engineering, National University of Singapore, 4 Engineering Drive 4, Singapore 117585, [§]Institute of Materials Research and Engineering, A*STAR (Agency for Science, Technology and Research), 3 Research Link, Singapore 117602, [∥]Department of Chemistry, Division of Biomedical Engineering, Hong Kong University of Science and Technology, Clear Water Bay, Kowloon, Hong Kong, China, and [⊥]Department of Chemistry, National University of Singapore, 3 Science Drive 3, Singapore 117543. [⊗]These authors (D.D. and D.M.) contributed equally.

ABSTRACT Monitoring and understanding long-term fate and regenerative therapy of administrated stem cells *in vivo* is of great importance. Herein we report organic nanodots with aggregation-induced emission characteristics (AIE dots) for long-term tracking of adipose-derived stem cells (ADSCs) and their regenerative capacity in living mice. The AIE dots possess high fluorescence (with a high quantum yield of 25 ± 1%), excellent biological and photophysical stabilities, low *in vivo* toxicity, and superb retention in living ADSCs with negligible interference on their pluripotency and secretome. These AIE dots also exhibit superior *in vitro* cell tracking capability compared to the most popular commercial cell trackers, PKH26 and Qtracker 655. *In vivo* quantitative studies with bioluminescence and GFP labeling as the controls reveal that the AIE dots can precisely and quantitatively report the fate of ADSCs and their regenerative capacity for 42 days in an ischemic hind limb bearing mouse model.

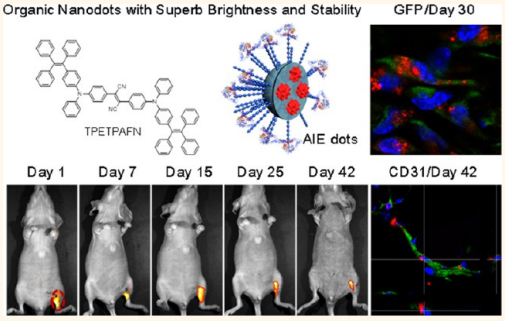

KEYWORDS: organic nanodots · adipose-derived stem cells · stem cell tracking · regenerative capacity · aggregation-induced emission

Stem cells are undifferentiated biological cells that are able to differentiate into specialized cells.[1,2] Among various stem cell sources, adipose-derived stem cells (ADSCs) possess rich promise as cell-based regenerative medicine, as they can be easily isolated from the stromal vascular fraction and exhibit extensive differentiation potential with easy expanding ability.[3,4] With the development of efficient stem cell therapies, it is of paramount importance to track the fate and regenerative capability of the administrated stem cells in both experimental models and clinical trials over a long period of time. Long-term, continuous, and precise *in vivo* stem cell tracing would provide clinicians and scientists with valuable information on monitoring of stem cell therapy, optimization of cell administration conditions, as well as assessment of treatment efficacy.[5−7]

In general, two main strategies have been explored for stem cell tracking. One is to mark the cells with reporter genes[8,9] and the other is to label the cells with exogenous contrast agents or imaging probes.[10] The reporter gene labeling approach offers veracious and quantitative information on the distribution and proliferation of stem cells *via* positron emission tomography (PET) or optical imaging.[11,12] Unfortunately, this approach is difficult to implement clinically due to several factors such as the requirements for transfection of genetic material and DNA modification of the cell population as well as the epigenetic gene silencing owing to DNA methylation, which may lead to raised concern of insertional mutagenesis,

* Address correspondence to tangbenz@ust.hk, kongdeling@nankai.edu.cn, cheliub@nus.edu.sg.

Received for review September 30, 2014 and accepted November 21, 2014.

Published online November 26, 2014
10.1021/nn505554y

adverse cellular effects, and suppressed reporter signals.[10,13−15] On the other hand, several imaging techniques along with exogenous contrast agents have been established for stem cell tracking. For instance, iron oxide nanoparticles are the most widely used exogenous agents for tracking of transplanted stem cells *via* magnetic resonance imaging (MRI), although low sensitivity and a time-dependent decrease in MRI signal have been reported.[6,10,16−18]

Among different imaging techniques, fluorescence imaging holds the advantages of high sensitivity, good temporal resolution, large *in vitro* and *in vivo* throughputs, and manoeuvrable imaging instruments.[10,19−21] Until now, organic dyes[22] and inorganic quantum dots (QDs)[23−26] have been widely utilized as stem cell trackers. Organic dyes, however, are limited by low photobleaching thresholds and facile leakage from cytoplasm to media.[27,28] Compared with organic dyes, QDs show more intense fluorescence, stronger photobleaching resistance, and longer retention time in living cells, which are highly regarded as promising candidates for tracking stem cells.[14,29] So far, many reported QDs suffer from intrinsic cytotoxicity caused by oxidative degradation of the heavy metal components,[30] inclination to aggregate in biological systems,[31] as well as irregular blinking phenomena,[32] which limit their applications in stem cell tracking. As a consequence, alternative fluorescent probes with superb optical properties and excellent cellular retention that can also overcome the limitations of QDs are urgently in demand for long-term stem cell tracking in living systems.

Very recently, fluorogens with aggregation-induced emission (AIE) characteristics have attracted increasing attention in biomedical applications.[33] AIE fluorogens are propeller-shaped molecules with rotor units such as phenyl rings, which are not fluorescent in solution. However, the fluorogens change to highly emit when aggregated as a result of restriction of the intramolecular motion.[34−37] Of particular interest are the AIE fluorogen-loaded organic dots, which have shown high cellular retention, robust biocompatibility, and flexible surface functionalization.[38,39] In addition, different from traditional dye-loaded nanoparticles, which show aggregation-caused quenching (ACQ) effect for dye aggregates,[40] the unique feature of AIE fluorogens opens up new opportunities for the fabrication of high loading organic dots with strong fluorescence.

To the best of our knowledge, a number of challenges still exist for the currently available exogenous contrast agents in *in vivo* long-term stem cell tracking. For example, considerably less effort has been focused on whether the agents can truly report the fate of stem cells *in vivo* after administration for an extremely long time and how the stem cells contribute to the regenerative therapy by taking advantage of the cell labeling. These may be hampered by either the relatively low resolution of imaging modality or the limited biological and photophysical stabilities of contrast agents. Moreover, many fluorescent probes are not good candidates for noninvasive monitoring of stem cells in living animals due to their relatively low brightness. Consequently, the unique features of AIE fluorogens motivate us to develop them into stem cell trackers to specifically address the aforementioned challenges. In this paper, we report the synthesis of QD-sized AIE dots with bright far-red/near-infrared (FR/NIR) fluorescence for noninvasive *in vivo* long-term tracking of ADSCs in an animal model of ischemia hind limb. The intense emission in the FR/NIR region and the large Stokes shift (∼160 nm) render the AIE dots suitable for *in vivo* imaging with low disturbed absorption, minimum background fluorescence, and deep tissue penetrability.[41] The brightness and photostability of AIE dots were assessed through single nanoparticle imaging. After evaluation of their *in vivo* toxicity, the AIE dots were utilized as exogenous fluorescent probes for *in vitro* and *in vivo* long-term ADSC tracking, which showed superior cell tracking performance to the most popular commercial cell trackers (*e.g.*, PKH 26 and Qtracker 655). Detailed experiments also revealed that the AIE dots internalization by the ADSCs did not affect their pluripotency, secretome, and *in vivo* treatment efficacy. More importantly, the AIE dots were demonstrated to be able to precisely track the ADSCs and their regenerative capacity, which provided us insight into understanding how ADSCs contributed to the ischemia therapy.

RESULTS AND DISCUSSION

The FR/NIR-emissive AIE fluorogen 2,3-bis(4-(phenyl-(4-(1,2,2-triphenylvinyl)phenyl)amino)phenyl)fumaronitrile (TPETPAFN) was synthesized[42] and demonstrated to hold AIE signature (Figure S1, Supporting Information). The AIE dots were fabricated through a modified nanoprecipitation method[43] using 1,2-distearoyl-*sn*-glycero-3-phosphoethanolamine-*N*-[(polyethylene glycol)-2000]-maleimide (DSPE-PEG2000-maleimide) as the encapsulation matrix. The TPETPAFN loading content in AIE dots was determined to be 39.8%, which ensured high brightness of the dots. The obtained AIE dots had surface maleimide groups, which were further modified with cell-penetrating peptide (derived from HIV-1 transactivator of transcription (Tat) protein) through maleimide−thiol coupling reaction in water in order to improve the cellular uptake of the dots. On average, there are ∼3800 Tat peptides conjugated on each AIE dot, which is described in detail in the Supporting Information. The chemical structure of TPETPAFN and the schematic illustration of AIE dot are shown in Figure 1A. Under transmission electron microscopy (TEM), the AIE dots show a spherical shape with a mean diameter of

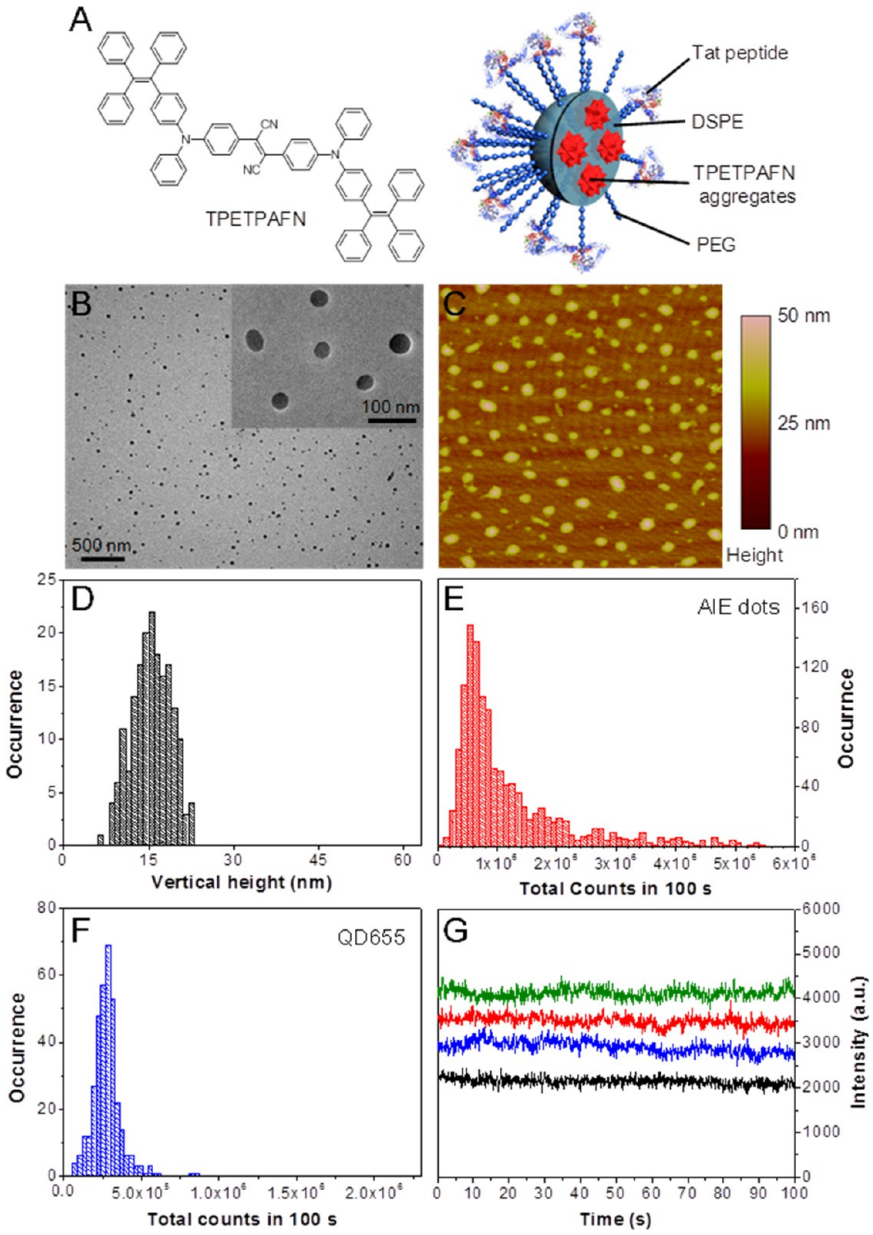

Figure 1. Structure of the AIE fluorogen and properties of the AIE dots used in this study. (A) Chemical structure of TPETPAFN and schematic illustration of the AIE dot. (B) TEM image of the AIE dots. The inset shows the enlarged TEM image. (C) AFM height image of the AIE dots. (D) Histogram of the AIE dot heights obtained from AFM (200 individual AIE dots were analyzed). Histograms of the total number of photons collected during 100 s for each of the (E) 1216 individual AIE dots and (F) 300 individual QD655. (G) Fluorescence time-traces of four individual AIE dots with different brightness levels.

~35 nm (Figure 1B). Figure 1C shows the atomic force microscopy (AFM) height image of AIE dots. Quantitative analysis based on 200 AIE dots indicates that the average vertical height distribution of the dots ranges from 6 to 22 nm with a peak at 16 nm (Figure 1D). The size of AIE dots hardly changed upon incubation in PBS buffer within a 3-week study duration, revealing their good stability. In addition, the AIE dots have absorption and emission maxima at 510 and 670 nm in water with a high quantum yield of 25 ± 1% measured using rhodamine 6G in ethanol as the reference (Figure S2, Supporting Information). The large Stokes shift of ~160 nm is beneficial for bioimaging with minimal background interference.[44]

Single nanoparticle fluorescence imaging of the obtained AIE dots was carried out upon excitation at 488 nm using commercially available QD655 (with a hydrodynamic size of ~28 nm, including the polymeric protective shell) as the reference. A total of 1216 AIE dots were analyzed to obtain the statistical histogram of the total photons emitted from the dots during 100 s, as shown in Figure 1E. The arithmetic average number of the total photons emitted by each AIE dot is approximately 1.18×10^6 counts per 100 s, which is on average ~4 times larger than that of QD655 (Figure 1F),

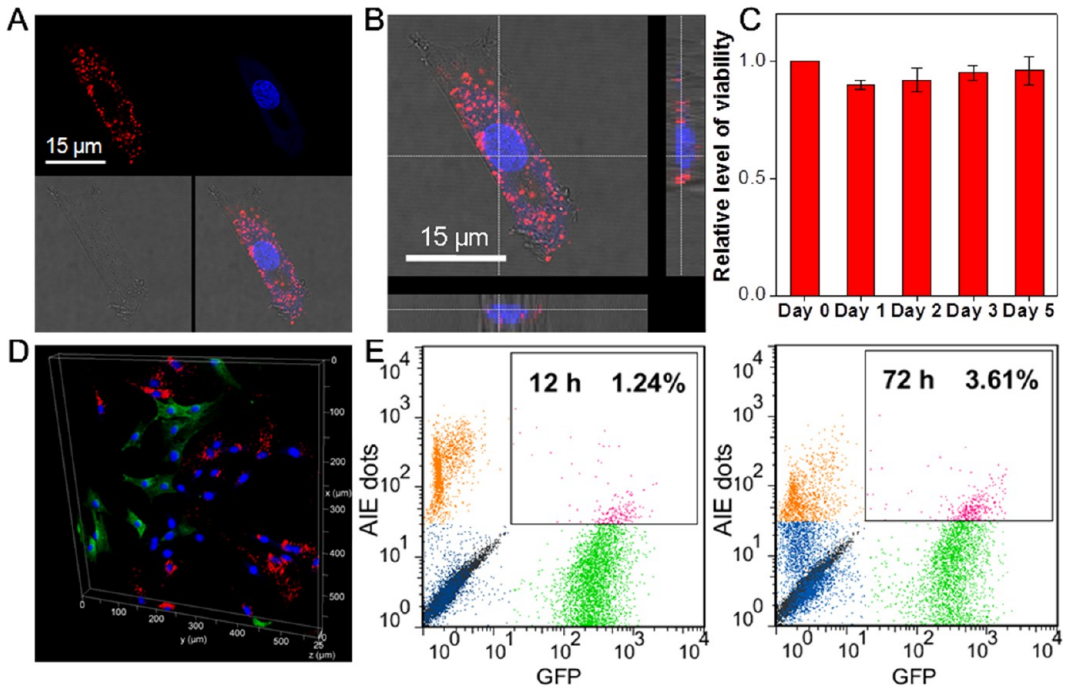

Figure 2. Fluorescence imaging and viability of ADSCs labeled by AIE dots: (A) confocal laser scanning microscopy (CLSM) images of an AIE dot-labeled ADSC; (B) 3D sectional CLSM image of the cell in (A); (C) metabolic viability of ADSCs after incubation with AIE dots (5 nM) for various time intervals; (D) 3D CLSM image of AIE dot-labeled ADSCs cocultured with green fluorescent protein (GFP)-expressed ADSCs for 3 days; (E) flow cytometry data of AIE dot-labeled and GFP-expressed ADSCs cocultured for 12 and 72 h. The cellular nuclei were stained by 4′,6-diamidino-2-phenylindole (DAPI, blue) in (A), (B), and (D).

indicating the higher brightness of each individual AIE dot. In addition, the intensity time-traces of four representative individual AIE dots were also obtained (Figure 1G), which revealed excellent photostability of the dots with negligible photobleaching during the observation period. More importantly, the AIE dots have stable emission without fluorescence intermittency, often referred to as "blinking",[32] which is of high importance in real-time single dot tracking.

Before stem cell tracking experiments, the *in vivo* toxicity of AIE dots was evaluated. A 0.1 mL portion of 100 nM AIE dots (the dot concentration is 100 times as that used for stem cell tracking) was intravenously injected into each healthy mouse, which was followed by monitoring of their distribution and metabolization in the mice over time. Figure S3A in the Supporting Information shows the time-dependent *in vivo* distribution profile in mice and *ex vivo* tissue imaging. Strong fluorescence is seen in the liver and spleen tissues post 3 h injection, indicating that the AIE dots are chiefly enriched in the reticuloendothelial system (RES) organs.[45] No detectable fluorescence was observed in any tissue of mice at day 9 postinjection, revealing that the AIE dots were able to be excreted from the body through the biliary pathway,[46] which was evidenced by the clear fluorescent signals in the collected feces but not urine (Figure S4, Supporting Information). Moreover, there is no noticeable body weight loss for the AIE dot-treated mice relative to that for the untreated control group (Figure S3B, Supporting Information). In fact, all the AIE dot-treated mice presented an active state in terms of movement, spirit, and skin luster.

Subsequently, a series of blood chemistry tests in terms of liver function, heme regulation, and red/white blood cell counts were performed 9 days after treatments. The results shown in Figure S3C (Supporting Information) reveal that no physiologically significant difference exists between AIE dot-treated and untreated groups. Finally, the histological analyses of important normal organs including liver, spleen, and kidney from AIE dot-treated mice were conducted as well. As shown in Figure S3D (Supporting Information), hematoxylin and eosin (H&E)-stained slices assessed by three independent pathologists suggest that the AIE dots hardly lead to any significative lesions to the normal organs. These data reveal that the AIE dots are safe for *in vivo* application.

The utility of AIE dots in stem cell labeling was investigated with confocal laser scanning microscopy (CLSM). After incubation with AIE dots (1 nM) at 37 °C for 4 h, the ADSCs were imaged by CLSM with 543 nm laser excitation, and the fluorescent signals were collected above 560 nm. Under the imaging conditions, no autofluorescence from the unlabeled ADSCs can be detected (Figure S5, Supporting Information). As shown in Figure 2A,B, the CLSM images along with the 3D sectional view show that obvious red fluorescence is observed in the ADSC cytoplasm, indicating that the AIE dots can be internalized into the cells for

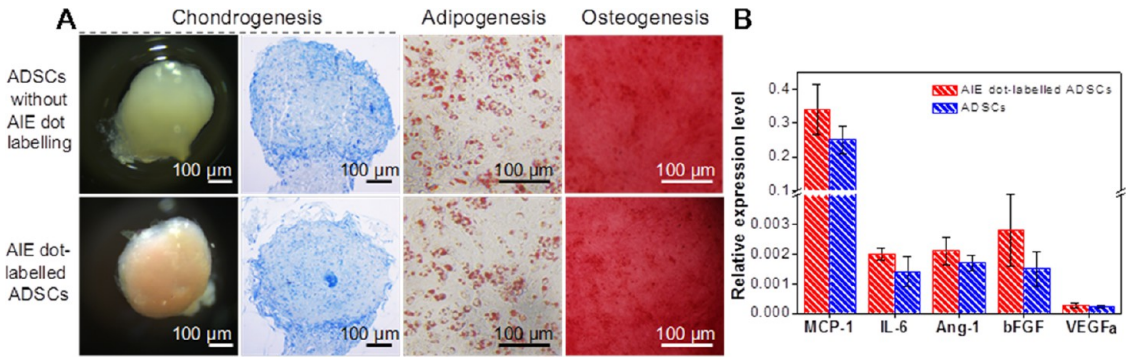

Figure 3. Effect of AIE dots on pluripotency and secretome of ADSCs: (A) chondrogenic, adipogenic, and osteogenic differentiation capacities as well as (B) secretome analyses of ADSCs with and without AIE dot labeling.

labeling. The *in vitro* cytotoxicity of AIE dots against ADSCs was then estimated using MTT cell-viability assays. Figure 2C depicts the cell viabilities after incubation with AIE dots at a dot concentration of 5 nM for up to 5 days. The cell viability remains >90% within 5-day study duration, indicating low cytotoxicity and good biocompatibility of AIE dots to ADSCs.

It is essential for exogenous labeling agents to possess excellent retention in living cells during cell proliferation.[16,28] To study whether the internalized AIE dots would leak from the intracellular compartments to the extracellular media, AIE dot-labeled ADSCs (without transfection of any reporter genes) were cocultured with green fluorescent protein (GFP)-expressed ADSCs. After coincubation for designated time intervals, the cells were examined by CLSM and flow cytometry. As shown in Figure 2D, the colocalization between red fluorescence from AIE dots and green fluorescence from GFP is hardly observed in any ADSC even after being cocultured for 3 days, which is also quantitatively verified by the corresponding flow cytometry data (Figure 2E). Similar results were also obtained when AIE dot-labeled ADSCs were cocultured with a GFP-expressed 4T07 breast cancer cell line (Figure S6, Supporting Information). These results reveal that the internalized AIE dots have very good retention in ADSCs, which are promising for long-term stem cell tracking.

We next studied whether the AIE dot internalization would influence the pluripotency of ADSCs. As shown in Figure 3A, the AIE dot-labeled ADSCs are capable of transforming into chondrogenic, adipogenic, and osteogenic cell lines, as evidenced by mast cells *via* toluidine blue staining,[47] the lipid-containing vacuoles in cells *via* oil-red O staining,[48] and mineralization of the ADSCs *via* Alizarin red S staining,[49] respectively. Noteworthy is that for each kind of differentiation no significant difference with respect to intensity and distribution of stain is found between cells labeled with and without AIE dots. These data indicate that the AIE dot internalization neither impacts the pluripotency of ADSCs nor causes any unintended differentiation.

The secretome behaviors of AIE dot-labeled ADSCs and control cells were investigated *via* quantitative real-time polymerase chain reaction (qPCR) measurements. As shown in Figure 3B, the levels of paracrine cytokines, including monocyte chemoattractant protein-1 (MCP-1), interleukin-6 (IL-6), angiopoietin-1 (Ang-1), basic fibroblast growth factor (bFGF), and vascular endothelial growth factor a (VEGFa), do not show a significant difference between AIE dot-labeled and unlabeled ADSCs. This result verifies that the AIE dot labeling does not obviously affect the secretome behavior of ADSCs.

The applications of the AIE dots in *in vitro* and *in vivo* ADSC tracking were subsequently investigated. The capacity of AIE dots for *in vitro* ADSC tracing was demonstrated first, using the most popular commercial cell trackers of PKH26[50] and Qtracker 655[51] as the references. The applied concentrations of AIE dots and Qtracker 655 were fixed at 1 nM. It should be noted that PKH26 cannot efficiently label the ADSCs at such a low concentration, and the recommended working concentration (2 μM) of PKH26 was used in this study. After labeling with each cell tracker, the ADSCs were subcultured for 1−5 days, and the cell fluorescence was subsequently studied by CLSM (Figure 4A) and flow cytometry (Figures S7 and S8, Supporting Information). Upon 1 day subculture, obvious fluorescent signals are observed for all the labeled ADSCs. Quantitative analyses of the CLSM images on day 1 using Image Pro Plus software indicate that the mean fluorescence intensity from AIE dot-labeled ADSCs is ~6.2 and ~4.8-fold higher than that from Qtracker 655- and PKH26-labeled ones, respectively. This result is in good agreement with the corresponding flow cytometry data. Furthermore, the flow cytometry result on day 1 also reveals that the ADSC labeling rates for AIE dots, PKH26, and Qtracker 655 are 98.5%, 97.5%, and 80.6%, respectively (Figure S7, Supporting Information). As shown in Figure 4A, after 5 day subculture, only weak fluorescence is detectable in Qtracker 655- (labeling rate of 12.4%) and PKH26-labeled (labeling rate of 43.9%) ADSCs, while intense and homogeneous fluorescent signals are still observed for AIE dot-labeled ones with

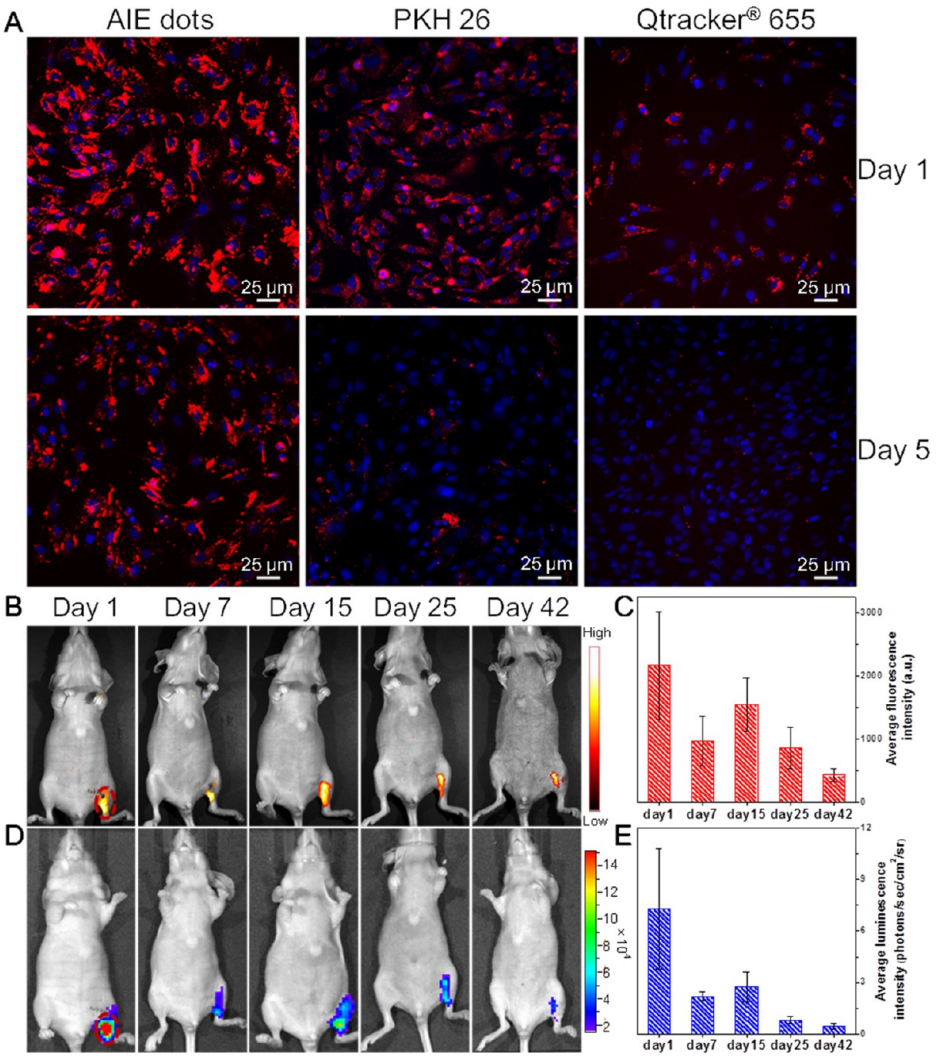

Figure 4. Long-term tracking of ADSCs *via* AIE dots. (A) CLSM images of ADSCs labeled with AIE dots, PKH26 as well as Qtracker 655 and then subcultured for 1 and 5 days, respectively. (B) Representative time-dependent *in vivo* fluorescence images of the ischemic hind limb-bearing mouse that was intramuscularly injected with AIE dot-labeled ADSC-containing Matrigel ($n = 8$ for this experiment). (C) Time-dependent fluorescence intensity changes for the region of interest (ROI: the cell transplanted site, which is indicated by red circle in (B)). (D) Representative time-dependent *in vivo* bioluminescence images of the same mouse in (B). (E) Time-dependent bioluminescence intensity changes for the ROI (indicated by red circle in (D)). The cellular nuclei were stained by DAPI (blue) in (A).

a labeling rate of 92.5% (Figure S8, Supporting Information). As PKH26 and Qtracker 655 have been reported as long-term stem cell tracers,[22,50−53] the superior performance of AIE dots in *in vitro* ADSC tracking makes them promising for *in vivo* monitoring of the stem cells.

The *in vivo* stem cell tracking ability of the AIE dots was examined on a hind limb ischemia model, utilizing the noninvasive live animal fluorescence imaging technique. It is worth pointing out that the ADSCs used in this study were isolated from the abdominal and inguinal adipose tissue of 8−12 week old male FVB-luc-GFP transgenic mice, which can express both luciferase and GFP for bioluminescence and fluorescence imaging, respectively. Therefore, the *in vivo* localization of the live ADSCs in mice could be noninvasively imaged through injection of a solution of luciferase substrate (D-luciferin). This will help to confirm whether AIE dots can precisely trace the fate of ADSCs in the living system and provide a good reference to further evaluate the ability of AIE dots for *in vivo* ADSC tracking. In addition, Matrigel was used as matrix to encapsulate the ADSCs for *in vivo* transplantation in order to improve the cell retention and survival at the injected site in mice.

After the ischemic hind limb was intramuscularly injected with AIE dot-labeled ADSC-containing Matrigel, the mice were imaged at designated time intervals. At each time point, the mice were simultaneously imaged using *in vivo* fluorescence as well as bioluminescence imaging systems. For fluorescence imaging, spectral unmixing with the Maestro software was utilized to get rid of the mouse background fluorescence (Figure S9, Supporting Information). Figure 4B

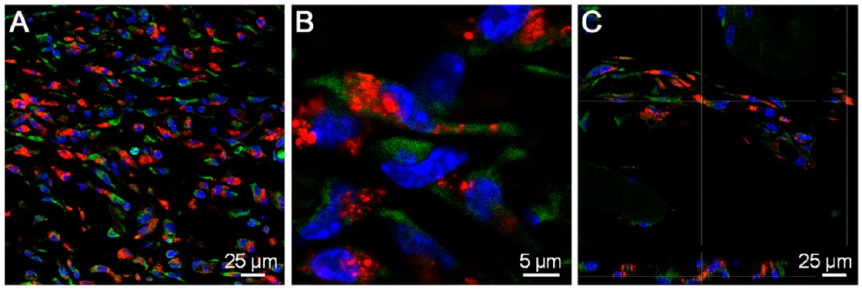

Figure 5. Tracking of ADSCs *in vivo* at single-cell resolution: (A) representative CLSM image of ischemic hind limb slices from mice after administration of AIE dot-labeled ADSC-containing Matrigels for 30 days; (B) enlarged CLSM image in A; (C) representative 3D sectional CLSM image taken on day 42. The green fluorescence in (A−C) is from GFP in the transplanted ADSCs. The cellular nuclei were stained by DAPI (blue).

shows the time-dependent distribution profile of the transplanted AIE dot-labeled ADSCs in living mice. Rortis fluorescence is seen in the hind limb post 1 h injection (day 1). As the time elapses, the fluorescent signals gradually decrease, but are still clearly distinguishable at the transplanted site for 42 days. Quantitative analyses of the fluorescent signals for the transplanted AIE dot-labeled ADSCs reveal a nearly continuous decrease in fluorescence intensity over time (Figure 4C). The same mice used for fluorescence imaging were also performed for bioluminescence imaging at the same time. As shown in Figure 4D, the pattern of live ADSC distribution in the hind limb is similar to that for fluorescence imaging at each time point. Furthermore, the trend of bioluminescence intensity alteration (Figure 4E) is almost the same as that for fluorescence imaging (Figure 4C). It is also noted that the transplanted ADSCs with and without AIE dot labeling exhibit similar bioluminescence signal intensity within 42 days, demonstrating that the AIE dot internalization has negligible influence on bioluminescence imaging of ADSCs (Figure S10, Supporting Information). As reporter gene labeling strategy is known for its accuracy and quantification in living cell tracking applications,[13] these data verify that the AIE dots can precisely and quantitatively report the fate of ADSCs in living mice.

Furthermore, on days 30 and 42, the mice transplanted with AIE dot-labeled ADSC-containing Matrigels were sacrificed and the ischemic hind limbs were dissected and sliced for CLSM observation. As the ADSCs in this study express GFP as well, it is convenient for us to estimate the accuracy of AIE dots in tracking ADSCs *in vivo* at single-cell resolution. As shown in Figure 5A,B, the CLSM images reveal that post 30-day ADSC administration, the fluorescent signals from AIE dots (red) and GFP (green) overlap well in the cytoplasma of most transplanted ADSCs. Quantitative analysis on day 30 based on 10 CLSM images from different fields of ischemic hind limb for each mouse (n = 4) indicates that ~86% of GFP-expressed ADSCs are stained with AIE dots. The good coincidence of AIE dot and GFP fluorescence in the same ADSCs is also observed (~78% of GFP-expressed ADSCs containing AIE dots *via* quantitative analyze) even after transplantation of the stem cells *in vivo* for 42 days (Figure 5C). The single-cell costain analysis further confirms the long-term ADSC tracking ability of AIE dots.

The research on the utility of ADSCs as therapeutic agents for ischemic diseases has attracted considerable attention.[3,4,54] As a consequence, it is critical to understand whether the cell trackers would influence the regenerative capability and therapeutic efficacy of ADSCs *in vivo*. To understand the effect of AIE dots on ADSC treatment efficacy, AIE dot-labeled and unlabeled ADSC-containing Matrigels (AIE dot-ADSC-M and ADSC-M in short) were intramuscularly transplanted into ischemic hind limbs of mice, respectively. The treatment efficacies of bare Matrigel transplantation and saline injection were also examined as controls. After 30 days postadministration, laser Doppler imaging analyses were carried out to assess the blood perfusion at the wound site for all the treatment groups. As shown in Figure 6A, significant vascularization with subcutaneous blood flows can be observed in the hind limbs of mice treated with AIE dot-ADSC-M and ADSC-M, whereas the foot and even the limb of the mice in bare Matrigel and saline groups are lost, resulting from the severe ischemia. The representative photographs showing the hind limbs of mice with different treatments are illustrated in Figure 6B. The blood flow of hind limb in the ischemic model was analyzed for all the treatment groups. On day 30, the perfusion ratios for AIE dot-ADSC-M and ADSC-M groups are similar, which are higher than those for the two control groups (Figure 6C).

Additionally, as compared to the control groups of bare Matrigel and saline injections, both ADSC treatments with and without AIE dot labeling significantly improved the percentages of limb salvage and reduced the percentages of foot necrosis and amputation post 42 days administration (Figure 6D). The H&E and immunohistochemical staining were also conducted on day 42. As shown in Figure 6E, typical H&E image of the ischemic limb in the saline injection group shows muscle degeneration in the ischemic region.

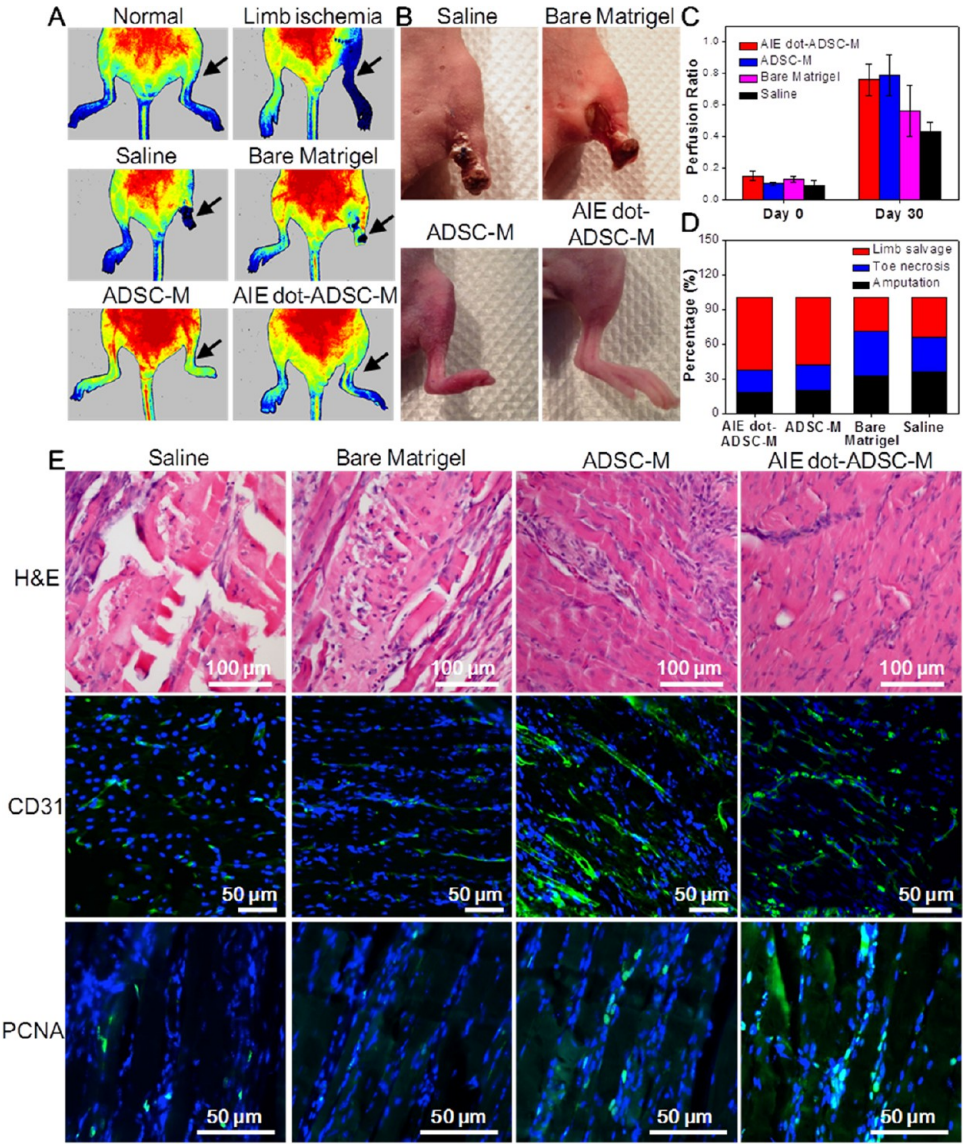

Figure 6. Impact of AIE dot labeling on ADSC therapy. (A) Laser Doppler perfusion images and (B) the representative photographs of the ischemic hind limb-bearing mice after 30 days post treatment. (C) Quantitative analysis of perfusion recovery determined by laser Doppler imaging. (D) Determination of limb salvage, toe necrosis, and limb loss of mice receiving different treatments on day 42. (E) H&E-, CD31-, and PCNA-staining images of ischemic hind limbs from mice after 42 days post treatment. The green fluorescence indicates the CD31-positive blood vessels or PCNA-positive nuclei in (E). The cellular nuclei were stained by DAPI (blue) in (E).

Transplantation of bare Matrigel attenuates muscle degeneration to some extent but fails to retain the large muscle fibrils as observed in the normal tissue (Figure S11, Supporting Information). In contrast, the ischemic limbs from mice treated with ADSC-M and AIE dot-ADSC-M display substantially reduced muscle degeneration with maximum fibrosis. In addition, both the AIE dot-ADSC-M and ADSC-M groups show significantly elevated density of CD31-positive blood vessels and increased number of proliferation active cells with proliferating cell nuclear antigen (PCNA)-positive nuclei in ischemic limbs as compared to the two control groups (Figure 6E and Figure S12, Supporting Information). These results suggest that ADSCs possess a great regenerative angiogenic potential and their transplantation is very effective in curing hind limb ischemia. In addition, AIE dot internalization does not affect the *in vivo* treatment efficiency of ADSCs.

We next investigated the utility of AIE dot labeling in understanding how ADSCs contribute to the ischemia therapy. The *in vivo* secretome behavior of AIE dot-labeled ADSCs was first studied by immunostaining against VEGF and bFGF. Figure 7A,B show the CLSM images of ischemic hind limb slices from mice after transplantation of AIE dot-labeled ADSC-containing Matrigels for 14 days. A close relativity in terms of the colocalization of the AIE dot-labeled cells (red fluorescence) with VEGF and bFGF (green fluorescence in Figure 7A,B, respectively) is observed from the slices, demonstrating that AIE dot-labeled ADSCs have *in vivo*

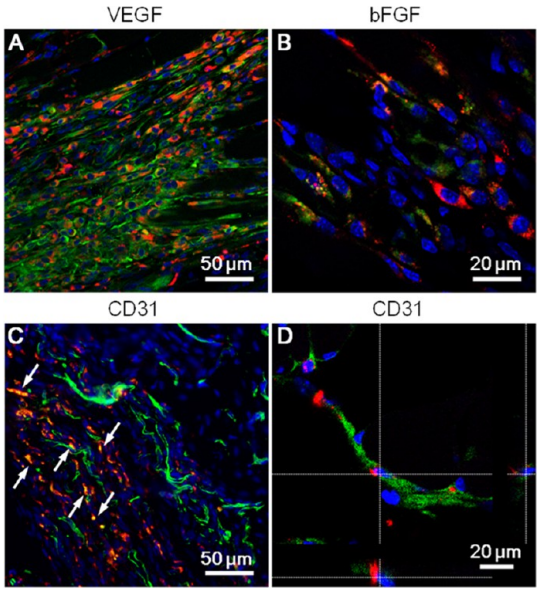

Figure 7. Long-term tracking of the regenerative capacity of ADSCs *via* AIE dots. Representative CLSM images of ischemic hind limb slices from mice after administration of AIE dot-ADSC-M for 14 days. The slices were immunostained against (A) VEGF and (B) bFGF, respectively. (C) Representative CD31-staining CLSM image and (D) 3D sectional CLSM image of ischemic hind limb slices from mice treated with AIE dot-ADSC-M for 42 days. The white arrows in (C) indicate the overlay yellow or orange fluorescence. The green fluorescence indicates the VEGF in (A), bFGF in (B), and CD31-positive blood vessels in (C and D). The cellular nuclei were stained by DAPI (blue).

regenerative ability by secreting angiogenic factors in the ischemic tissue. In comparison, the VEGF and bFGF fluorescent signals are significantly decreased in the slices from mice treated with saline or bare Matrigel (Figure S13, Supporting Information), confirming the *in vivo* secretory capability of AIE dot-labeled ADSCs. Furthermore, upon blood vessel staining against CD31 on day 42, it is found that most AIE dot-labeled ADSCs (red fluorescence) are distributed near or close to the CD31-positive blood vessels (green fluorescence, Figure 7C), indicating the induction of therapeutic angiogenesis *via* the cells. More importantly, as shown in Figure 7C, several AIE dot-labeled cells are located in the blood vessels, especially in the capillaries, as evidenced by the overlay yellow or orange fluorescence. The enlarged 3D sectional CLSM image depicted in Figure 7D verifies that the AIE dot-labeled ADSCs can also participate in blood vessel formation through forming vascular structures. Therefore, by taking advantage of AIE dot labeling, we conclude that the ADSCs are contributing to the angiogenesis in ischemic tissue *via* not only secreting angiogenic factors, such as VEGF and bFGF, but also differentiating into necessary cells *in vivo* to participate in neovascularisation. These data also illustrate that the AIE dots are able to track and visualize the regenerative capacity of ADSCs in a long-term manner.

CONCLUSIONS

In summary, we have developed AIE dots with ultrahigh stability and brightness, explored their applications in noninvasive long-term tracking of ADSCs, and monitored their regenerative capability in an ischemic hind limb model. The prepared AIE dots show very low *in vivo* toxicity and excellent photostability with negligible photobleaching in single nanoparticle fluorescence imaging. The AIE dot labeling is found to have negligible interference on the pluripotency and secretome of the ADSCs. The *in vitro* ADSC tracing experiments reveal that the AIE dots possess superb retention within the ADSCs and have superior *in vitro* cell tracking ability over commercially available cell trackers, Qtracker 655 and PKH26. The ADSC tracking studies in mice bearing ischemic hind limbs demonstrate that the AIE dots can precisely and quantitatively report the fate of ADSCs and their regenerative capacity *in vivo* for 6 weeks. To the best of our knowledge, the 6-week observation represents the longest *in vivo* cell tracking duration among the currently available exogenous fluorescent cell trackers, indicating that the AIE dots are unique fluorescent probes for long-term cell tracking.

Similar to other exogenous stem cell trackers, AIE dots have shown advantages such as good biocompatibility, high cellular retention, simple labeling procedure and high throughput. In addition, the AIE dots also have their own uniqueness: (1) as compared to traditional organic fluorophores that undergo fluorescence quenching upon aggregation, the aggregation-induced emission characteristics of AIE fluorogens offer new opportunities to synthesize nanodots with high loading and bright fluorescence; (2) the AIE dots can track the stem cells *in vivo* for 6 weeks, not only in a noninvasive manner but also with single-cell resolution; (3) the AIE dots are capable of precisely and quantitatively report the fate of ADSCs *in vivo*, which is validated by simultaneous reporter gene imaging; (4) more importantly, the AIE dots are demonstrated to be able to long-term track the regenerative capability of ADSCs in ischemic tissues. Noteworthy is that very little work has focused on tracking the regenerative capacity of stem cells using cell trackers.[14,20] An impressive work by Yu's group has utilized fluorescent nanodiamonds to label lung stem cells, which was able to monitor the cells and their regenerative ability *in vivo* for 7 days.[20]

It is noted that QD-based fluorescent probes have been reported as an important class of cell trackers available for advancing the stem cell field.[16] The superior *in vitro* and *in vivo* performance of AIE dots in stem cell tracking clearly verifies their great potentials in practice. Moreover, as compared to the reporter gene labeling strategy (*e.g.*, luciferase-labeling method) that is difficult to envision clinically and only widely used in

small animals,[7,13−15] the AIE dot-labeling approach is simple, inexpensive, safe, and effective, which holds great promise for potential clinical translation. Considering the remarkable advantages of AIE dots over other fluorescent probes in terms of brightness, photostability, safety, and ADSC tracking ability, this successful example of long-term *in vivo* tracking of stem cells and their regenerative capacity will inspire more exciting research in this emerging field.

EXPERIMENTAL SECTION

Materials. 1,2-Distearoyl-*sn*-glycero-3-phosphoethanolamine-*N*-[(polyethylene glycol)-2000]-maleimide (DSPE-PEG_{2000}-maleimide) was obtained from Laysan Bio, Inc. (Arab, AL). HIV-1 transactivator of transcription (Tat) protein-derived cell penetrating peptide (C-terminus with cysteine) was purchased from GL Biochem Co., Ltd. (Shanghai, China). Qtracker 655 cell labeling kit was purchased from Life Technologies, Invitrogen (Singapore). TranZol Reagent was provided by TransGen Biotechnology Inc. (Beijing, China). Matrigel Matrix was purchased from BD Biosciences Inc. (Franklin Lakes, NJ). Other chemicals were bought from Sigma-Aldrich. 2,3-Bis(4-(phenyl(4-(1,2,2-triphenylvinyl)phenyl)amino)phenyl)fumaronitrile (TPETPAFN) was synthesized on the basis of our previous report.[42]

Characterization. UV−vis and emission spectra were measured using a Shimadzu UV-1700 spectrometer and PerkinElmer LS 55 spectrofluorometer, respectively. Transmission electron microscopy (TEM, JEM-2010F, JEOL, Japan) and atomic force microscopy (AFM, Veeco Bioscope II microscope equipped with a NanoScope IIIa controller) were employed to investigate the sample morphology. For AFM measurement, a drop of dilute solution of the nanodots was added onto a clean glass cover slide.

Preparation of AIE Dots. TPETPAFN (1 mg) and DSPE-PEG_{2000}-maleimide (1.5 mg) were dissolved in 1 mL of tetrahydrofuran (THF). Accompanied by sonication by a microtip probe sonicator (12 W output, XL2000, Misonix Incorporated, NY), the above THF solution was added into 9 mL of water, which was followed by further sonication for 60 s. The suspension was stirred in the fume hood at room temperature for 12 h in order to remove the THF. Afterward, the AIE dot suspension was performed for ultrafiltration (molecule weight cutoff 100 kDa) at 3000 g for 30 min. A 0.2 μm syringe driven filter was then employed to further purify the dot suspension. The amount of TPETPAFN aggregates successfully encapsulated into the DSPE-PEG_{2000}-maleimide matrix was estimated by the absorption spectra utilizing a calibration curve of THF solutions of TPETPAFN as the reference. The TPETPAFN loading content in AIE dots is defined as the ratio of fluorogen mass incorporated in the dots to the total mass of the AIE dots. To conjugate Tat peptides on the AIE dots, 1 μmol of peptide was added into the AIE dot suspension, which was allowed to react for 12 h. The free Tat peptide was subsequently removed by ultrafiltration.

Cell Culture. Luciferase+/GFP+ ADSCs were isolated from the abdominal and inguinal adipose tissue of 8−12 weeks old male FVB-luc-GFP transgenic mice and subsequently cultured and expanded in 10 cm^2 plate in complete growth medium containing α-Minimum Essential Medium supplemented with 20% fetal bovine serum (FBS) and 100 U/mL of penicillin-streptomycin at 37 °C in a humidified environment containing 5% CO_2. The culture medium was changed twice a week. The ADSCs of passages 3 were used for all of the experiments in this work.

***In Vitro* ADSC Tracking.** DSCs (2×10^6) were seeded in a 6 cm^2 plate and cultured at 37 °C. After removal of the medium and washing with 1× PBS buffer, the ADSCs were exposed to 1 nM AIE dots for 4 h at 37 °C. After that, the cells were washed twice with culture medium, detached by 1 × tripsin, and then subcultured for 1 and 5 days, respectively. The cells subcultured for different time periods were imaged by CLSM (Leica TSC SP8, Germany) with excitation at 543 nm and signal collection >560 nm. The fluorescence intensities of AIE dot-labeled ADSCs were then assessed by flow cytometry (Becton Dickinson, San Jose, CA) measurements. Ten thousand events were counted for each sample to plot the histogram (λ_{ex} = 488 nm, 680/20 nm bandpass filter). The *in vitro* ADSC tracking studies *via* PKH26 (2 μM) and Qtracker 655 (1 nM) were also performed following the same procedures.

Animals and Ischemia Hind Limb Model. All animal studies were performed under the guidelines set by the Tianjin Committee of Use and Care of Laboratory Animals, and the overall project protocols were approved by the Animal Ethics Committee of Nankai University. Eight weeks old female BALB/c nude mice (obtained from the Laboratory Animal Center of the Academy of Military Medical Sciences (Beijing, China)) were used to set up the ischemia hind limb model. Briefly, after anesthetization of the mice, the left femoral artery and vein were ligated *via* a skin incision with 7-0 silk and cut from just above the deep femoral artery to the popliteal artery and vein.

Tracking of ADSCs in Living Mice. The ADSCs were first labeled with AIE dots (1 nM) as above-mentioned. AIE dot-labeled ADSCs (1×10^6) were encapsulated in 30 μL of Matrigel, which were then intramuscularly injected into the ischemic hind limbs of female BALB/c nude mice. The Maestro EX fluorescence imaging system (CRi, Inc.) was utilized to image the mice (n = 8) by placing the anesthetized mice on the equipped platform (λ_{ex} = 523 nm, signal collection: 560 to 900 nm (10 nm step), exposure time = 200 ms, scans: day 1, 7, 15, 25, and 42 postinjection, respectively). Maestro software was used to remove the mouse background fluorescence. Furthermore, at the same time points of fluorescence imaging, bioluminescence imaging was performed using the Xenogen IVIS Lumina II system as well. Briefly, D-luciferin (150 mg/kg) was intraperitoneally injected into the AIE dot-labeled ADSC-administrated mice (the same mice used for fluorescence imaging). The mice were then imaged by receiving 1 s to 5 min scans. The bioluminescence signals were quantified in units of maximum photons per second per square centimeter per steridian. Bioluminescence imaging was conducted by a technician who did not know the project conditions.

***In Vivo* Regenerative Therapy Efficacy.** The ischemic hind limb-bearing mice were randomly assigned to four groups and intramuscularly injected with saline (n = 5), bare Matrigels (n = 5), AIE dot-labeled ADSC-containing Matrigels (AIE dot-ADSC-M; n = 8), and unlabeled ADSC-containing Matrigels (ADSC-M; n = 6), respectively. Laser Doppler imaging was conducted to quantitatively detect the subcutaneous blood flow of hind limbs using a PeriCam PSupporting Information System (Perimed AB, Sweden) on day 0 and 30 postinjection. The average values of perfusion were subsequently determined. In addition, on day 42 postinjection, the percentages of limb salvage, toe necrosis, and amputation in each treatment group were also quantified.

Statistical Analysis. Quantitative data were expressed as mean ± standard deviation. ANOVA analysis and Student's t test were utilized for statistical contrast. $P < 0.05$ was figured statistically significant.

Conflict of Interest: The authors declare no competing financial interest.

Supporting Information Available: Experimental section and figures depicting optical properties, *in vivo* toxicity, flow cytometry histograms of various cell tracker-labeled ADSCs subcultured for 1 and 5 days, bioluminescence images of mouse injected with unlabeled ADSCs, as well as quantitative analyses of ischemic hind limb slices from mice after 42 days post different treatments. This material is available free of charge *via* the Internet at http://pubs.acs.org.

Acknowledgment. This work was supported by the National Basic Research Program of China (2011CB964903), the PCSIRT (IRT13023), the NSFC (81301311 and 81220108015), the Singapore National Research Foundation (R-279-000-390-281), the Singapore-MIT Alliance for Research and Technology (SMART) Innovation Grant (R279-000-378-592), the A*STAR Joint Council Office and Institute of Materials Research and Engineering of Singapore (IMRE/13-8P1104), and the Research Grants Council of Hong Kong (HKUST/CRF/10 and N_HKUST620/11).

REFERENCES AND NOTES

1. Jiang, Y.; Jahagirdar, B. N.; Reinhardt, R. L.; Schwartz, R. E.; Keene, C. D.; Ortiz-Gonzalez, X. R.; Reyes, M.; Lenvik, T.; Lund, T.; Blackstad, M.; *et al.* Pluripotency of Mesenchymal Stem Cells Derived from Adult Marrow. *Nature* **2002**, *418*, 41–49.
2. Reya, T.; Morrison, S. J.; Clarke, M. F.; Weissman, I. L. Stem Cells, Cancer, and Cancer Stem Cells. *Nature* **2001**, *414*, 105–111.
3. Gimble, J. M.; Katz, A. J.; Bunnell, B. A. Adipose-Derived Stem Cells for Regenerative Medicine. *Circ. Res.* **2007**, *100*, 1249–1260.
4. Miranville, A.; Heeschen, C.; Sengenès, C.; Curat, C. A.; Busse, R.; Bouloumié, A. Improvement of Postnatal Neovascularisation by Human Adipose Tissue-Derived Stem Cells. *Circulation* **2004**, *110*, 349–355.
5. Frangioni, J. V.; Hajjar, R. J. *In Vivo* Tracking of Stem Cells for Clinical Trials in Cardiovascular Disease. *Circulation* **2004**, *110*, 3378–3383.
6. Xu, C. J.; Miranda-Nieves, D.; Ankrum, J. A.; Matthiesen, M. E.; Phillips, J. A.; Roes, I.; Wojtkiewicz, G. R.; Juneja, V.; Kultima, J. R.; Zhao, W.; *et al.* Tracking Mesenchymal Stem Cells with Iron Oxide Nanoparticle Loaded Poly(Lactide-co-Glycolide) Microparticles. *Nano Lett.* **2012**, *12*, 4131–4139.
7. Jokerst, J. V.; Khademi, C.; Gambhir, S. S. Intracellular Aggregation of Multimodal Silica Nanoparticles for Ultrasound-Guided Stem Cell Implantation. *Sci. Transl. Med.* **2013**, *5*, 117ra35.
8. Brader, P.; Serganova, I.; Blasberg, R. G. Noninvasive Molecular Imaging Using Reporter Genes. *J. Nucl. Med.* **2013**, *54*, 167–172.
9. Cao, F.; Lin, S.; Xie, X.; Ray, P.; Patel, M.; Zhang, X.; Drukker, M.; Dylla, S. J.; Connolly, A. J.; Chen, X.; et al. *In Vivo* Visualization of Embryonic Stem Cell Survival, Proliferation, and Migration after Cardiac Delivery. *Circulation* **2006**, *113*, 1005–1014.
10. Kircher, M. F.; Gambhir, S. S.; Grimm, J. Noninvasive Cell-Tracking Methods. *Nat. Rev. Clin. Oncol.* **2011**, *8*, 677–688.
11. McCracken, M. N.; Gschweng, E. H.; Nair-Gill, E.; McLaughlin, J.; Cooper, A. R.; Riedinger, M.; Cheng, D.; Nosala, C.; Kohn, D. B.; Witte, O. N. Long-Term *In Vivo* Monitoring of Mouse and Human Hematopoietic Stem Cell Engraftment with a Human Positron Emission Tomography Reporter Gene. *Proc. Natl. Acad. Sci. U.S.A.* **2013**, *110*, 1857–1862.
12. Bhaumik, S.; Gambhir, S. S. Optical Imaging of Renilla Luciferase Reporter Gene Expression in Living Mice. *Proc. Natl. Acad. Sci. U.S.A.* **2002**, *99*, 377–382.
13. Nguyen, P. K.; Riegler, J.; Wu, J. C. Stem Cell Imaging: From Bench to Bedside. *Cell Stem Cell* **2014**, *14*, 431–444.
14. Ransohoff, J. D.; Wu, J. C. Imaging Stem Cell Therapy for the Treatment of Peripheral Arterial Disease. *Curr. Vasc. Pharmacol.* **2012**, *10*, 361–373.
15. Gu, E.; Chen, W. Y.; Gu, J.; Burridge, P.; Wu, J. C. Molecular Imaging of Stem Cells: Tracking Survival, Biodistribution, Tumorigenicity, and Immunogenicity. *Theranostics* **2012**, *2*, 335–345.
16. Ferreira, L.; Karp, J. M.; Nobre, L.; Langer, R. New Opportunities: The Use of Nanotechnologies to Manipulate and Track Stem Cells. *Cell Stem Cell* **2008**, *3*, 136–146.
17. Guzman, R.; Uchida, N.; Bliss, T. M.; He, D.; Christopherson, K. K.; Stellwagen, D.; Capela, A.; Greve, J.; Malenka, R. C.; Moseley, M. E.; *et al.* Long-Term Monitoring of Transplanted Human Neural Stem Cells in Developmental and Pathological Contexts with MRI. *Proc. Natl. Acad. Sci. U.S.A.* **2007**, *104*, 10211–10216.
18. Nam, T.; Park, S.; Lee, S. Y.; Park, K.; Choi, K.; Song, I. C.; Han, M. H.; Leary, J. J.; Yuk, S. A.; Kwon, I. C.; *et al.* Tumor Targeting Chitosan Nanoparticles for Dual-Modality Optical/MR Cancer Imaging. *Bioconjugate Chem.* **2010**, *21*, 578–582.
19. Kondepati, V. R.; Heise, H. M.; Backhaus, J. Recent Applications of Near-Infrared Spectroscopy in Cancer Diagnosis and Therapy. *J. Anal. Bioanal. Chem.* **2008**, *390*, 125–139.
20. Wu, T. J.; Tzeng, Y. K.; Chang, W. W.; Cheng, C. A.; Kuo, Y.; Chien, C. H.; Chang, H. C.; Yu, J. Tracking the Engraftment and Regenerative Capabilities of Transplanted Lung Stem Cells Using Fluorescent Nanodiamonds. *Nat. Nanotechnol.* **2013**, *8*, 682–689.
21. Li, J. L.; Goh, C. C.; Keeble, J. L.; Qin, J. S.; Roediger, B.; Jain, R.; Wang, Y.; Chew, W. K.; Weninger, W.; Ng, L. G. Intravital Multiphoton Imaging of Immune Responses in the Mouse Ear Skin. *Nat. Protocols* **2012**, *7*, 221–234.
22. Sutton, E. J.; Henning, T. D.; Pichler, B. J.; Bremer, C.; Daldrup-Link, H. E. Cell Tracking with Optical Imaging. *Eur. Radiol.* **2008**, *18*, 2021–2032.
23. Seleverstov, O.; Zabirnyk, O.; Zscharnack, M.; Bulavina, L.; Nowicki, M.; Heinrich, J. M.; Yezhelyev, M.; Emmrich, F.; O'Regan, R.; Bader, A. Quantum Dots for Human Mesenchymal Stem Cells Labelling. A Size-Dependent Autophagy Activation. *Nano Lett.* **2006**, *6*, 2826–2832.
24. Solanki, A.; Kim, J. D.; Lee, K. B. Nanotechnology for Regenerative Medicine: Nanomaterials for Stem Cell Imaging. *Nanomedicine* **2008**, *3*, 567–578.
25. Lin, S.; Xie, X.; Patel, M. R.; Yang, Y. H.; Li, Z.; Cao, F.; Gheysens, O.; Zhang, Y.; Gambhir, S. S.; Rao, J. H.; *et al.* Quantum Dot Imaging for Embryonic Stem Cells. *BMC Biotechnol.* **2007**, *7*, 67–76.
26. Muller-Borer, B. J.; Collins, M. C.; Gunst, P. R.; Cascio, W. E.; Kypson, A. P. Quantum Dot Labelling of Mesenchymal Stem Cells. *J. Nanobiotechnol.* **2007**, *5*, 9.
27. Resch-Genger, U.; Grabolle, M.; Cavaliere-Jaricot, S.; Nitschke, R.; Nann, T. Quantum Dots *versus* Organic Dyes as Fluorescent Labels. *Nat. Methods* **2008**, *5*, 763–775.
28. Yu, Y.; Feng, C.; Hong, Y.; Liu, J.; Chen, S.; Ng, K. M.; Luo, K. Q.; Tang, B. Z. Cytophilic Fluorescent Bioprobes for Long-Term Cell Tracking. *Adv. Mater.* **2011**, *23*, 3298–3302.
29. Yang, K.; Li, Z.; Cao, Y.; Yu, X.; Mei, J. Effect of Peptide-Conjugated Near-Infrared Fluorescent Quantum Dots (NIRF-QDs) on the Invasion and Metastasis of Human Tongue Squamous Cell Carcinoma Cell Line Tca8113 *In Vitro*. *Int. J. Mol. Sci.* **2009**, *10*, 4418–4427.
30. Derfus, A. M.; Chan, W. C. W.; Bhatia, S. N. Probing the Cytotoxicity of Semiconductor Quantum Dots. *Nano Lett.* **2004**, *4*, 11–18.
31. Smith, A. M.; Duan, H.; Mohs, A. M.; Nie, S. M. Bioconjugated Quantum Dots for *In Vivo* Molecular and Cellular Imaging. *Adv. Drug Delivery Rev.* **2008**, *60*, 1226–1240.
32. Wu, C. F.; Bull, B.; Szymanski, C.; Christensen, K.; McNeill, J. Multicolor Conjugated Polymer Dots for Biological Fluorescence Imaging. *ACS Nano* **2008**, *2*, 2415–2423.
33. Ding, D.; Li, K.; Liu, B.; Tang, B. Z. Bioprobes Based on AIE Fluorogens. *Acc. Chem. Res.* **2013**, *46*, 2441–2453.
34. Hong, Y. N.; Lam, J. W. Y.; Tang, B. Z. Aggregation-Induced Emission. *Chem. Soc. Rev.* **2011**, *40*, 5361–5388.
35. Hong, Y. N.; Lam, J. W. Y.; Tang, B. Z. Aggregation-Induced Emission: Phenomenon, Mechanism and Applications. *Chem. Commun.* **2009**, 4332–4353.
36. Wang, M.; Zhang, G. X.; Zhang, D. Q.; Zhu, D. B.; Tang, B. Z. Fluorescent Bio/Chemosensors Based on Silole and Tetraphenylethene Luminogens with Aggregation-Induced Emission Feature. *J. Mater. Chem.* **2010**, *20*, 1858–1867.
37. Li, Z.; Dong, Y.; Mi, B.; Tang, Y.; Häussler, M.; Tong, H.; Dong, Y.; Lam, J. W. Y.; Ren, Y.; Sung, H. H. Y.; *et al.* Structure Control of the Photoluminescence of Silole Regioisomers and Their Utility as Sensitive Regiodiscriminating Chemosensors and Efficient Electroluminescent Materials. *J. Phys. Chem. B* **2005**, *109*, 10061–10066.
38. Li, K.; Zhu, Z.; Cai, P.; Liu, R.; Tomczak, N.; Ding, D.; Liu, J.; Qin, W.; Zhao, Z.; Hu, Y.; *et al.* Organic Dots with Aggregation-Induced

Emission (AIE dots) Characteristics for Dual-Color Cell Tracing. *Chem. Mater.* **2013**, *25*, 4181–4187.
39. Chen, M. J.; Yin, M. Z. Design and Development of Fluorescent Nanostructures for Bioimaging. *Prog. Polym. Sci.* **2014**, *39*, 365–395.
40. Birks, J. B. *Photophysics of Aromatic Molecules*; Wiley-Interscience: London, 1970.
41. Frangioni, J. V. *In Vivo* Near-Infrared Fluorescence Imaging. *Curr. Opin. Chem. Biol.* **2003**, *7*, 626–634.
42. Li, K.; Qin, W.; Ding, D.; Tomczak, N.; Geng, J.; Liu, R.; Liu, J.; Zhang, X.; Liu, H.; Liu, B.; *et al.* Photostable Fluorescent Organic Dots with Aggregation-Induced Emission (AIE dots) for Noninvasive Long-Term Cell Tracing. *Sci. Rep.* **2013**, *3*, 1150.
43. Li, K.; Jiang, Y.; Ding, D.; Zhang, X.; Liu, Y.; Hua, J.; Feng, S. S.; Liu, B. Folic Acid-Functionalized Two-Photon Absorbing Nanoparticles for Targeted MCF-7 Cancer Cell Imaging. *Chem. Commun.* **2011**, *47*, 7323–7325.
44. Gao, X. H.; Cui, Y. Y.; Levenson, R. M.; Chung, L. W. K.; Nie, S. M. *In Vivo* Cancer Targeting and Imaging with Semiconductor Quantum Dots. *Nat. Biotechnol.* **2004**, *22*, 969–976.
45. Peer, D.; Karp, J. M.; Hong, S.; Farokhzad, O. C.; Margalit, R.; Langer, R. Nanocarriers as an Emerging Platform for Cancer Therapy. *Nat. Nanotechnol.* **2007**, *2*, 751–760.
46. Liu, Z.; Davis, C.; Cai, W.; He, L.; Chen, X.; Dai, H. Circulation and Long-Term Fate of Functionalized, Biocompatible Single-Walled Carbon Nanotubes in Mice Probed by Raman Spectroscopy. *Proc. Natl. Acad. Sci. U.S.A.* **2008**, *105*, 1410–1415.
47. Yu, B.; Yu, D.; Cao, L.; Zhao, X.; Long, T.; Liu, G.; Tang, T.; Zhu, Z. Simulated Microgravity Using a Rotary Cell Culture System Promotes Chondrogenesis of Human Adipose-Derived Mesenchymal Stem Cells *via* the p38 MAPK Pathway. *Biochem. Biophys. Res. Commun.* **2011**, *414*, 412–418.
48. Choi, Y. S.; Cha, S. M.; Lee, Y. Y.; Kwon, S. W.; Park, C. J.; Kim, M. Adipogenic Differentiation of Adipose Tissue Derived Adult Stem Cells in Nude Mice. *Biochem. Biophys. Res. Commun.* **2006**, *345*, 631–637.
49. Bagnaninchi, P. O.; Drummond, N. Real-Time Label-Free Monitoring of Adipose-Derived Stem Cell Differentiation with Electric Cell-Substrate Impedance Sensing. *Proc. Natl. Acad. Sci. U.S.A.* **2011**, *108*, 6462–6467.
50. Lanzkron, S. M.; Collector, M. I.; Sharkis, S. J. Hematopoietic Stem Cell Tracking *In Vivo*: A Comparison of Short-Term and Long-Term Repopulating Cells. *Blood* **1999**, *93*, 1916–1921.
51. Fischer, U. M.; Harting, M. T.; Jimenez, F.; Monzon-Posadas, W. O.; Xue, H.; Savitz, S. I.; Laine, G. A.; Cox, C. S., Jr. Pulmonary Passage is a Major Obstacle for Intravenous Stem Cell Delivery: The Pulmonary First-Pass Effect. *Stem Cells Dev.* **2009**, *18*, 683–692.
52. Tang, D. G. Understanding Cancer Stem Cell Heterogeneity and Plasticity. *Cell Res.* **2012**, *22*, 457–472.
53. Srivastava, A. K.; Bulte, J. W. M. Seeing Stem Cells at Work. *In Vivo. Stem Cell Rev. Rep.* **2014**, *10*, 127–144.
54. Nakagami, H.; Maeda, K.; Morishita, R.; Iguchi, S.; Nishikawa, T.; Takami, Y.; Kikuchi, Y.; Saito, Y.; Tamai, K.; Ogihara, T.; *et al.* Novel Autologous Cell Therapy in Ischemic Limb Disease Through Growth Factor Secretion by Cultured Adipose Tissue-Derived Stromal Cells. *Arterioscler. Thromb. Vasc. Biol.* **2005**, *25*, 2542–2547.